

# Continued Functionality Performance for Base Isolated Structures Subjected to Earthquakes

**S. Chimamphant & K. Kasai**

*Tokyo Institute of Technology, Japan*

**T.A. Morgan**

*Exponent, Inc., USA*



## SUMMARY:

In order to study the performance of base isolated structures considering continued functionality, the PEER Performance Based Earthquake Engineering (PBEE) methodology is adopted. A continued functionality performance state is obtained from specific fragility functions for nonstructural components. MDOF linear response history analysis is utilized to investigate parametrically the performance of several combinations of isolation period, isolation damping ratio, and superstructure period. Sensitivities of these basic properties are described. Results indicate that having higher isolation period always improves the performance of the base isolated building, however increasing isolation damping ratio does not always improve the performance, especially in tall buildings. The performance is always worsened with the increase in superstructure height.

*Keywords: Continued Functionality, Performance, Base Isolated Structure, Nonstructural Component*

## 1. INTRODUCTION

Seismic isolation technology is an innovative approach of anti-seismic design of structures, which has been used widely in that last few years. There has been research on the performance of individual base isolation systems and their supported structure. However, very few studies focused on the performance of base isolation based on continued functionality (CF) of buildings. Therefore, the objectives of this study are to investigate the effects of isolation and superstructure properties on the response of base isolated structures and to study the performance of base isolated structures with several combinations of isolation and superstructure properties considering continued functionality (CF)

## 2. ANALYSIS MODEL

The analytical model for a generic MDOF system is represented in this study by a stick model. An example model representing a 3-story base isolated structure is shown in Fig. 2.1(a). The superstructure is assumed to have an inverted triangular mode shape as shown in the right figure of Fig. 2.1(b) regardless of how the base moves shown in the left figure of Fig. 2.1(b).

Assuming equal masses at each floor of the superstructure, and by defining the fundamental superstructure period  $T_s$  and the mode shape vector  $\phi$  of the superstructure, the stiffness for each story ( $k_1, k_2, \dots, k_n$ ) can be obtained by solving Eqn. 2.1:

$$\begin{pmatrix} \underline{K} - \frac{4\pi^2}{T_s^2} \underline{M} \\ \underline{K}_{n \times n} & \underline{M}_{n \times n} \end{pmatrix} \begin{pmatrix} \underline{\phi} \\ \underline{\phi}_{n \times 1} \end{pmatrix} = \begin{pmatrix} \underline{0} \\ \underline{0}_{n \times 1} \end{pmatrix} \quad (2.1)$$

where  $\underline{K}$  is stiffness matrix and  $\underline{M}$  is mass matrix. The superstructure period  $T_s$  is assumed to be  $0.1N_s$ , where  $N_s$  is the number of stories above the isolation level. Superstructure damping is proportional to

the stiffness matrix, and a damping ratio  $\zeta_s$  is assumed to be 2% in the first mode.

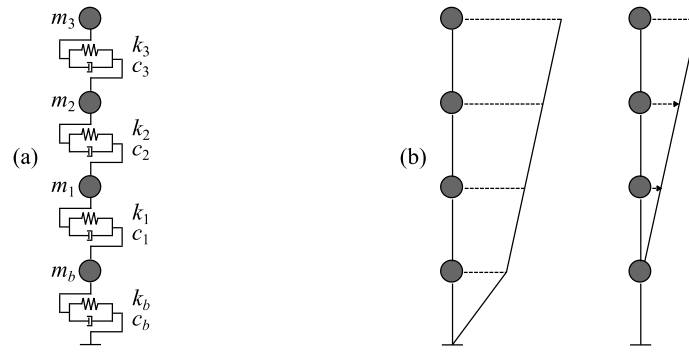


**Figure 2.1.** Model: (a) stick model (b) mode shape

Considering the base isolation system, with the assumption that the superstructure is rigid, we define the isolation period  $T_b$ , and isolation damping ratio  $\zeta_b$  in Eqn. 2.2 where  $m_b$  is mass at the base and  $m_i$  is mass at  $i^{\text{th}}$  floor.

$$T_b = 2\pi \sqrt{\frac{m_b + \sum_{j=1}^{N_s} m_j}{k_b}}, \quad \zeta_b = \frac{c_b T_b}{4\pi \left( m_b + \sum_{j=1}^{N_s} m_j \right)} \quad (2.2)$$

With the assumption that the drift demands are small according to the definition of continued functionality described in section 6.2, this continued functionality damage state is expected to be triggered under elastic deformations of the superstructure. As a result, linear elastic behaviour is assumed in the superstructure. Additionally, a linear viscous base isolation system is considered in the current study.

Masses in all floors are assumed equal to one, story heights are equal in all stories and are assumed to be equal to 350 cm. Twenty ground motions from Los Angeles SAC suite of ground motions for a 2% in 50 years seismic hazard (LA21 – LA40) are used in this study.

### 3. PARAMETRIC STUDY

To study the sensitivity of the performance to basic properties of base isolated structures, a variety of (1) base isolation periods  $T_b$ , (2) base isolation damping ratios  $\zeta_b$ , and (3) number of stories  $N_s$  are investigated as listed below:

- (1)  $T_b = \{ 2.0, 3.0, 4.0 \}$  seconds
- (2)  $\zeta_b = \{ 0.10, 0.30 \}$
- (3)  $N_s = \{ 3, 9, 20 \}$  stories

These base isolated structures are subjected to the 20 ground motions. The responses are described as median values with an assumption that these responses are lognormally distributed.

### 4. SENSITIVITY TO BASIC PROPERTIES

To study the natural behaviors of these base isolated structures and to investigate the various combinations of isolation properties and superstructure properties, these base isolated structures are subjected to real unscaled ground motions (LA21 – LA40).

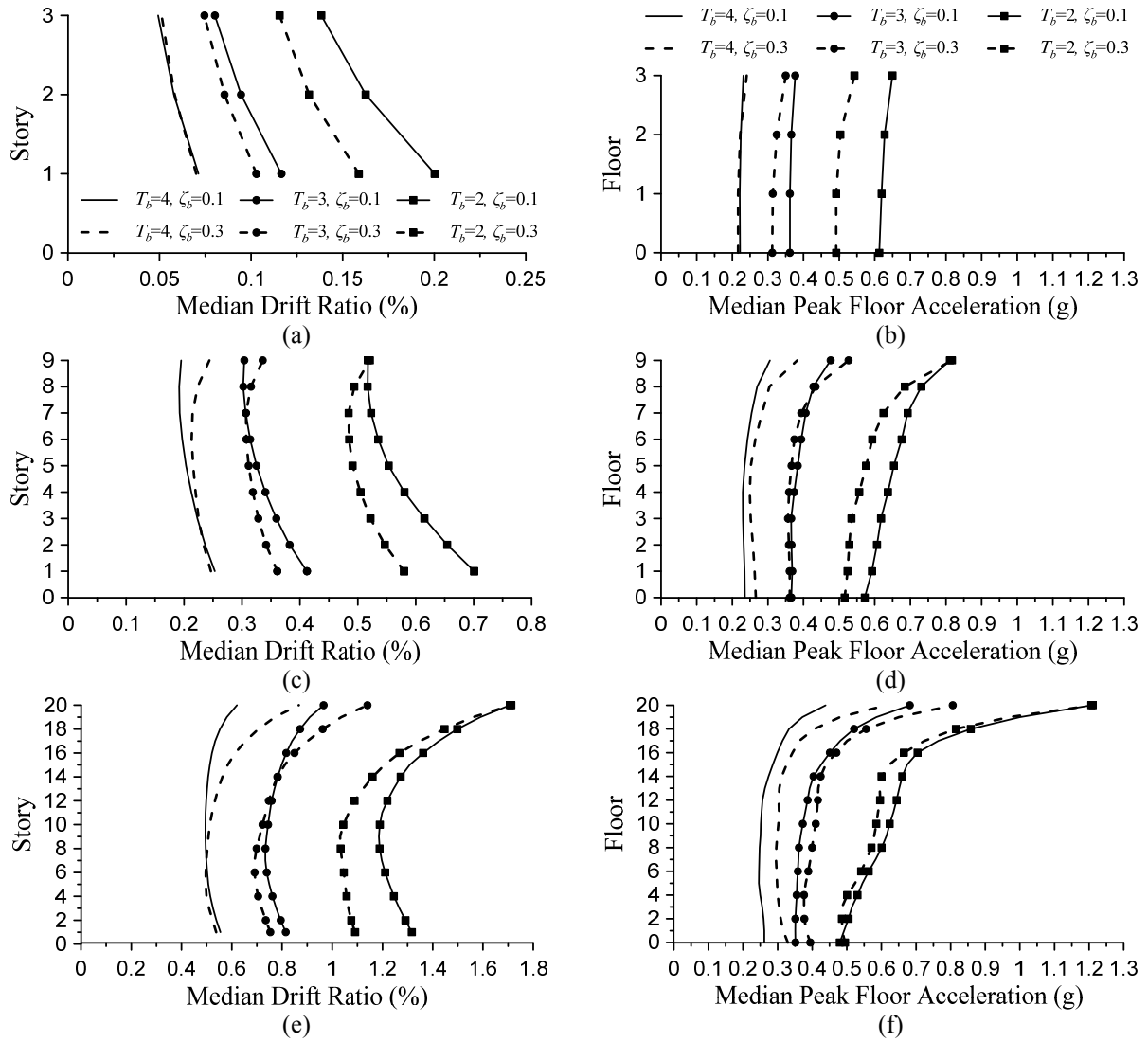


**Figure 4.1.** Median responses for (a,b) 3-story, (c,d) 9-story, and (e,f) 20-story base isolated structures

#### 4.1. Sensitivity to Base Isolation Period ( $T_b$ )

From Fig. 4.1, it can be clearly observed that an increase of isolation period  $T_b$  reduces both the drift and acceleration demands in superstructures of both stiff and flexible buildings regardless of isolation damping  $\zeta_b$ . This is unsurprising because an increase of the isolation period  $T_b$  is a reduction in the isolation stiffness resulting in concentration of drift demand in the base isolation level.

#### 4.2. Sensitivity to Base Isolation Damping Ratio ( $\zeta_b$ )

Examining the results described in Fig. 4.1, it can be observed that the distributions of both drift and acceleration demands are sensitive to isolation damping. For short buildings or stiff structures, the distribution is altered slightly, whereas for tall or flexible structures, the alteration of the distribution is more dramatic.

For higher isolation period  $T_b$ , there is tendency that added isolation damping ratio  $\zeta_b$  may reduce the demands in some floors and increase the demands in the others as can be seen in Fig. 4.1(b,c,e).

Results also reveal that added isolation damping  $\zeta_b$  could help reducing the demand in the superstructure when isolation period  $T_b$  is low, however, if  $T_b$  is high, added isolation damping  $\zeta_b$  could increase the demand in the superstructure as clearly seen in Fig. 4.1.

### 4.3. Sensitivity to Number of Stories ( $N_s$ )

Examining the drift demands in Fig. 4.1(a), it can be seen clearly that for short buildings, drift demands are very low when compared with taller buildings as shown in Fig. 4.1(c,e). This indicates that base isolation system works well for short buildings, as expected. For tall buildings, large drift demands become concentrated in upper stories. Increased acceleration demands also appear to be concentrated in the upper stories as clearly seen in Fig. 4.1(d,f).

## 5. MODE CONTRIBUTION

To investigate the contribution from higher modes, transfer functions are estimated for each analysis case by using Eqn. 5.1:

$$G(\omega) = \frac{A_{\text{output}}(\omega)}{A_{\text{input}}(\omega)} \quad (5.1)$$

where  $A_{\text{output}}$  is the acceleration at the top floor in the frequency domain and  $A_{\text{input}}$  is the acceleration at the ground in the frequency domain. The transfer functions shown subsequently are from the results of 3-, 9-, and 20-story base isolated structures, having  $T_b = 2, 3,$  and 4 seconds respectively, subjected to the same unscaled ground motion LA21. The results are shown in Fig. 5.1.

All peaks indicate natural periods for the base isolated structures. Observing mode contributions for the 9- and 20-story base isolated structures, the 2<sup>nd</sup> and 3<sup>rd</sup> modes seem to contribute significantly at the top floor. This indicates the significance of higher mode contributions in the base isolated structures. To further investigate the mode contributions in each floor, transfer functions are developed for selected floors in the 9-story base isolated structure as shown in Fig. 5.2.

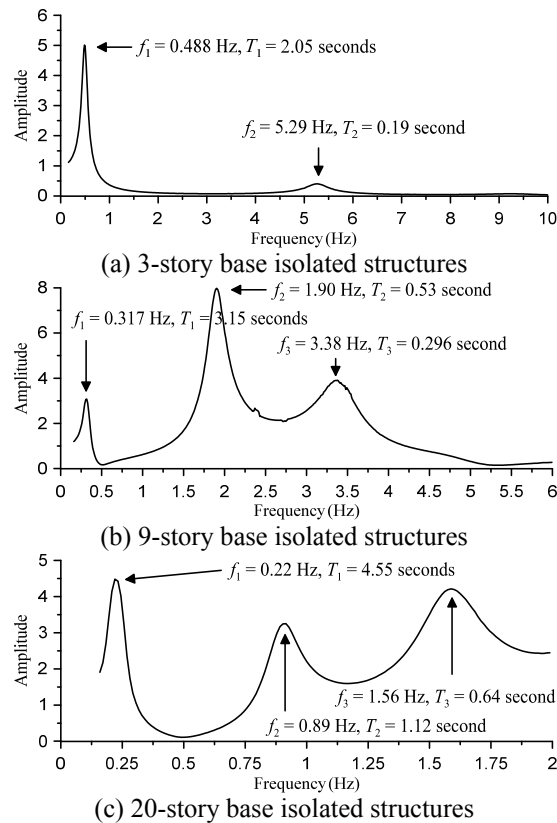


**Figure 5.1.** Transfer functions of base isolated structures between top floor and ground

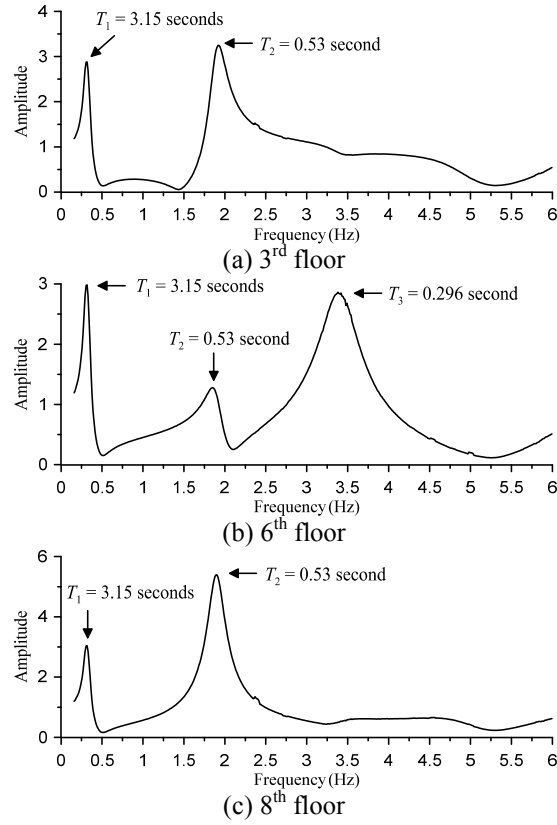


**Figure 5.2.** Transfer functions of 9-story base isolated structures between middle floors and ground

It appears that for the 3<sup>rd</sup> and 8<sup>th</sup> floors, the second mode gets excited more than the first mode, and the third has a negligible contribution. However, in the 6<sup>th</sup> floor, the third mode (whose period of 0.3 sec is close to the period of the ceiling) appears to be significant.

## 6. METHODOLOGY

### 6.1. Performance Based Earthquake Engineering

To study the effects of isolation system properties and superstructure properties on continued functionality ( $CF$ ), the PEER Performance Based Earthquake Engineering methodology is adopted.

The complete equation for calculating  $\lambda_{CF}$ , the annual probability that a base isolated structure exceeds the continued functionality of partition walls (or other drift-sensitive components), is shown in Eqn. 6.1.

$$\lambda_{CF} = \sum_{k=1}^n \left\{ P[dm > CF | \delta = \delta_k] \cdot \sum_{j=1}^m \left\{ P[\delta = \delta_k | S_a = \bar{S}_{a,j}] P[S_a = \bar{S}_{a,j}] \right\} \right\} \quad (6.1)$$

$P[dm > CF | \delta = \delta_k]$  is the probability of damage state  $dm$  exceeding continued functionality state  $CF$  for a specific drift ratio  $\delta$  and is determined from the damage fragility curve.

$P[\delta = \delta_k | S_a = \bar{S}_{a,j}]$  is the probability that a specific drift ratio  $\delta$  occurs for a specific ground motion intensity level  $S_a$  and is determined from drift distribution at each intensity level.

$P[S_a = \bar{S}_{a,j}]$  is the annual probability that a specific seismic intensity level  $S_a$  is observed at a specific site and is obtained directly from hazard curve corresponding to a specific site location and natural period of interest.

## 6.2. Definition of Continued Functionality

Continued functionality is the performance state in which a building remains usable without interruption after an earthquake. Hence, the damage that triggers this continued functionality state is very slight, corresponding to small values of drift ratio and floor acceleration.

## 7. FRAGILITY FUNTIONS

### 7.1. Fragility of Drift Sensitive Components

To represent drift sensitive components, fragility functions for partition walls are selected. Experiments on light gauge steel studded gypsum partition walls have been conducted recently at the University of Buffalo to assess their seismic fragility (Filiatrault et al. 2010). The fragility functions reported in their study is adopted here. The damage description corresponding to *CF* is “slight damage to partition walls.” For this damage state, the median drift ratio and dispersion are 0.35% and 0.56, respectively. Fig. 7.1(a) shows the fragility curve with the median and dispersion described above.

### 7.2. Fragility of Acceleration Sensitive Components

To represent acceleration sensitive components, fragility functions for suspended ceilings are selected. From recent work by Motoyui and Sato (2011), fragility of Japanese ceiling systems is obtained through Monte Carlo analysis using 2D finite element analysis and assumed statistical variation of the strength of connections from experimental testing. The period of the ceiling  $T_{ceiling}$  is 0.32 second. The fragility function describing “failure of ceiling” reported in their study is used. The median acceleration and dispersion are 0.505g and 0.046, respectively. Fig. 7.1(b) shows the fragility curve with the median and dispersion described above.

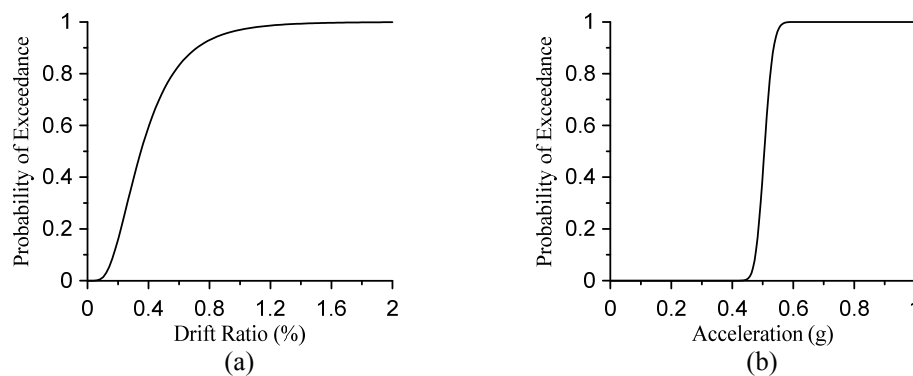


**Figure 7.1.** Damage fragility functions: (a) Partition walls (b) Suspended ceilings

## 8. SEISMIC HAZARD CURVE

The hazard curve can be obtained for a specific site location and a natural period of interest based on some attenuation model. In this study, the site is assumed to be located in downtown Los Angeles area. The hazard curve is then obtained using the attenuation model by Campbell and Bozorgnia (2008) with  $V_{S30} = 760$  m/s representing the boundary between B and C soil types, as defined in ASCE 7 (2005). Fig. 8.1 shows the hazard curves at the site for natural periods of 2, 3, and 4 seconds.

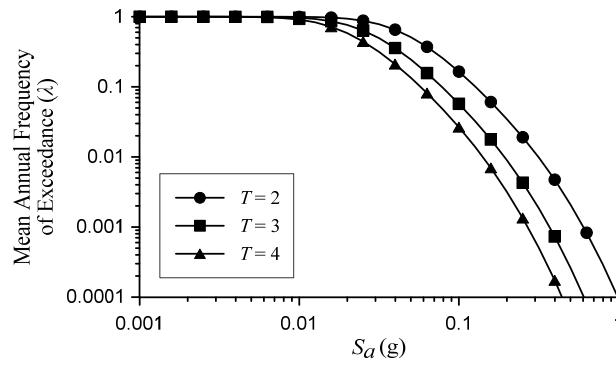


Figure 8.1. Hazard curves in Los Angeles Area

## 9. PERFORMANCE EVALUATION

In order to obtain the performance of a base isolated structure, three components are needed as described previously in section 6.1. These components are used concurrently as shown in Eqn. 6.1. The value obtained from this Equation is the mean annual frequency of exceedance the continued functionality damage state  $\lambda_{CF}$ . The expected return period  $TR$  (in years) can be calculated by taking reciprocal of  $\lambda_{CF}$  ( $TR = 1/\lambda_{CF}$ ).

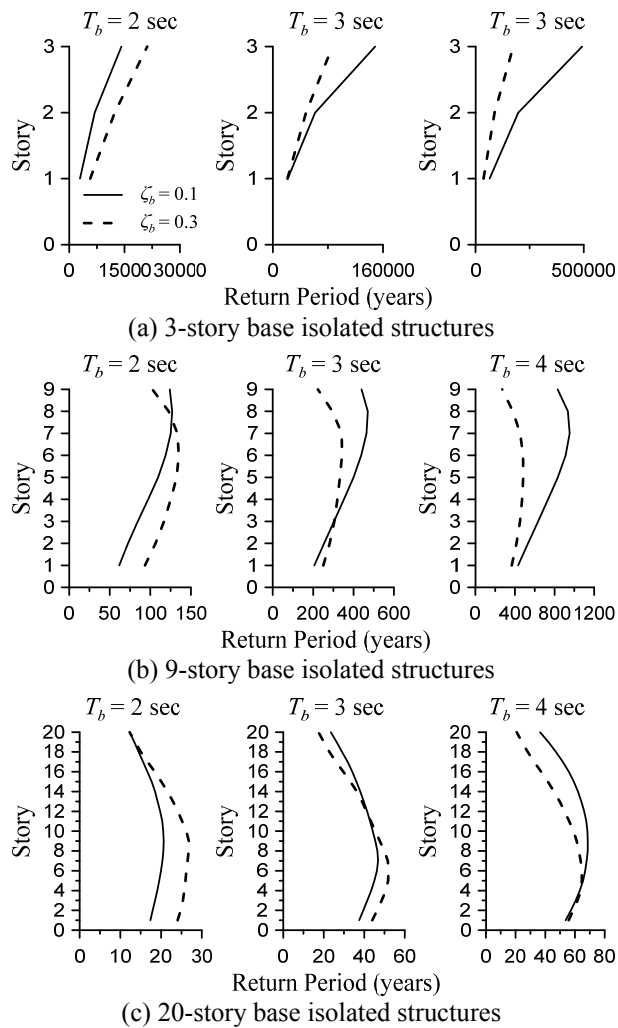
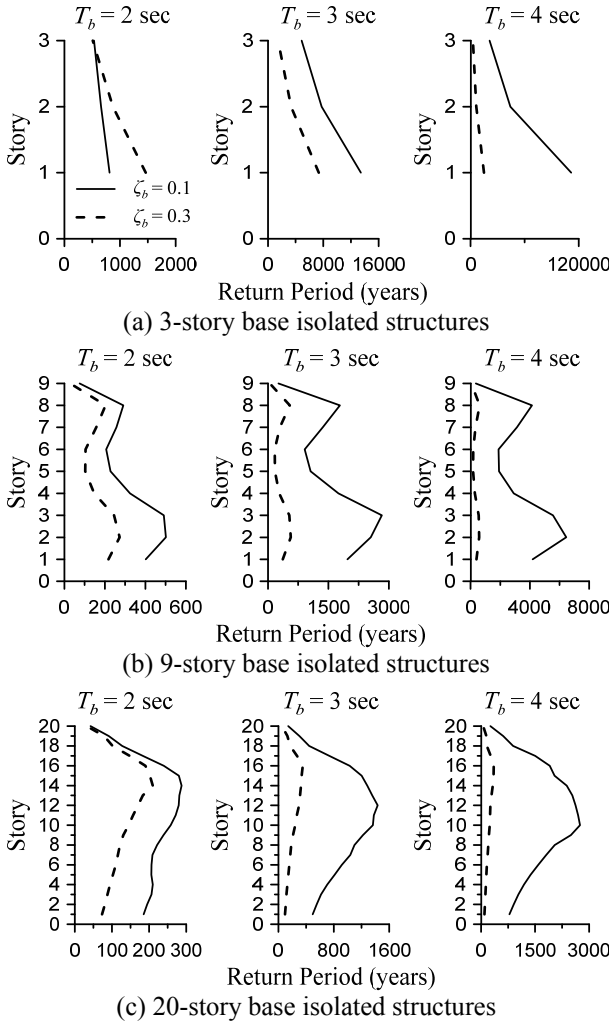


Figure 9.1. Performance in return period (years) based on the continued functionality damage state of partition walls

### 9.1. Performance Based on CF of Partition Walls

Examining the results described in Fig. 9.1, the performance in terms of return period  $TR$  in each floor corresponds well to the drift demands described in Fig. 4.1(a,c,e). Higher drift demands result in poorer performance, whereas lower drift demands result in better performance. Observing the expected return period  $TR$  for these isolated structures, it is seen clearly that the return periods in short buildings are significantly higher than tall buildings. This indicates that, considering drift sensitive components, isolation systems work well for short buildings. However, for tall buildings, the return period could be as low as around 10 years in the top story of 20-story base isolated structures, meaning that there is a high chance that some partition walls need to be fixed or replaced over the life of the building, resulting in interruption of the usage of this story due to wall repair or replacement.



**Figure 9.2.** Performance in return period (years) based on the continued functionality damage state of suspended ceilings

### 9.2. Performance Based on CF of Suspended Ceilings

From Fig. 9.2, the return period  $TR$  in each floor does not correspond well to the acceleration demands described in Fig. 4.1(b,d,f). This is because the performance calculated is based on the peak acceleration at the period of the ceiling,  $T_{ceiling} = 0.32$  sec, not the peak floor acceleration as shown in Fig. 4.1(b,d,f). There are also higher mode effects present in the 9- and 20-story base isolated structures.

Fig. 5.1(a) shows that the 3-story base isolated structure has dominant natural frequencies of 0.488 Hz and 5.29 Hz which are corresponding to the periods of 2.05 sec and 0.19 sec. Higher modes do not appear to be significant for this structure. However, in Fig. 5.1(b,c), the 2<sup>nd</sup> and 3<sup>rd</sup> modes can be clearly observed, particularly in Fig. 5.1(b). The 3<sup>rd</sup> mode period is 0.3 sec, which is close to the period of the ceiling  $T_{ceiling}$ . This will affect the performance of those stories whose significant modes are near the period of the ceiling. As a result, the performance distribution becomes more difficult to predict in taller buildings. Fig. 5.2 also shows clearly which floors are sensitive to the third mode, implying low performance if that mode is substantially excited. This explains why the performance of 9-story base isolated structures shown in Fig. 9.2(b) has such an irregular shape.

## 10. CONCLUSIONS

Results indicate that having higher isolation period  $T_b$  always improves the performance of the base isolated building, however increasing isolation damping ratio  $\zeta_b$  does not always improve the performance, especially in tall buildings. This is attributed to the excitation of higher mode effects due to non-proportional damping. Considering the superstructure height, the performance is always worsened as the height increases.

The performance considering drift sensitive components shows that isolation system works well on short/stiff structures. The performance becomes worse as the superstructure becomes more flexible. As for acceleration sensitive components, results for short buildings reveals that, due to their naturally stiff structures, the acceleration is high which results in poor performance. However, in tall buildings, due to their flexibility, the performance is improved. This indicates that for short isolated buildings, the performance is more sensitive to acceleration demand, whereas for tall isolated buildings, the performance is more sensitive to drift demand.

## ACKNOWLEDGEMENT

The authors acknowledge support from the Japan Ministry of Education, Culture, Sports, Science and Technology (MEXT) for establishing the Center for Urban Earthquake Engineering (CUEE) in Tokyo Institute of Technology. This support makes possible the forthcoming international conference, as well as international joint research projects and exchange programs with overseas universities.

## REFERENCES

- Campbell, K.W. and Bozorgnia, Y. (2008). NGA ground motion model for the geometric mean horizontal component of PGA, PGV, PGD and 5% damped linear elastic response spectra for periods ranging from 0.01 to 10 s. *Earthquake Spectra*. **24:1**, 139–171.
- Chopra, A. K. (2007). *Dynamics of Structures: Theory and Applications to Earthquake Engineering*, Prentice-Hall, Upper Saddle River, NJ.
- Moehle, J. and Deierlein, G. (2004). A Framework Methodology for Performance-Based Earthquake Engineering. *Proceedings of the 13<sup>th</sup> World Conference on Earthquake Engineering*. **Paper No: 679**
- Motoyui, S., Sato, Y., Macrae, G.A., Dhakal, R.P. (2011). Ceiling Fragility of Japanese Ceiling Systems. *Proceedings of the 9th Pacific Conference on Earthquake Engineering*.
- Retamales, R., Davies, R., Mosqueda, G., Filiatrault, A. (2010). Experimental Seismic Fragility Assessment of Light Gauge Steel Studded Gypsum Partition Walls. *9<sup>th</sup> U.S. National & 10<sup>th</sup> Canadian Conference on Earthquake Engineering*.
- Vamvatsikos, D., Cornell, C.A. (2001). Incremental Dynamic Analysis. *Earthquake Engineering & Structural Dynamics*. **31:3**, 491-514.